PCCP

PAPER

View Article Online
View Journal | View Issue

Cite this: *Phys. Chem. Chem. Phys.*, 2017, **19**, 1975

X-ray and molecular dynamics studies of butylammonium butanoate–water binary mixtures†

Umme Salma,*[a] Marianna Usula,[b] Ruggero Caminiti,[a] Lorenzo Gontrani,*[a] Natalia V. Plechkova[c] and Kenneth R. Seddon[c]

Received 6th October 2016,
Accepted 19th December 2016

DOI: 10.1039/c6cp06860j

www.rsc.org/pccp

The nanostructural organisation of mixtures of the ionic liquid (butylammonium butanoate) and water at several mole fractions of water has been investigated using small and wide angle X-ray scattering (S-WAXS) and molecular dynamics (MD) simulations. The presence of a first sharp diffraction peak (FSDP) in the pure ionic liquid has been observed, experimentally and theoretically, suggesting the possibility of segregation of domains of different polarity in the system. With increasing dilution in water, the prepeak is shifted towards smaller Q values, and becomes very weak, while the principal peak moves towards larger Q values. These phenomena suggest the disruption of the hydrogen-bonded network of the ionic liquid, primarily through hydrogen bonding of the anion to water, a conclusion supported by MD simulations.

Introduction

The burgeoning growth in interest in ionic liquids (ILs) is reflected in the large number of books, reviews and papers which have been published this century.[1] Particularly exciting is our increasing understanding of the intimate molecular structure of simple ionic liquids.[2,3] Over the last decade, imidazolium and alkylammonium ionic liquids have gained particular attention from researchers due to their intriguing spatial heterogeneity, which appears to be induced by the balance between their inherent polar/nonpolar regions.[4] Combined experimental and theoretical studies have been performed, showing the presence of a remarkable segregation structure with alkyl chains of intermediate to long length.[5] Seddon and co-workers reported experimental work in which a liquid crystal phase was observed for pure ionic liquids with long alkyl chain;[6,7] intermediate range order due to segregation of the alkyl chains was also reported for some protic ionic liquids by Greaves *et al.*[8] 1-Butyl-3-methylimidazolium halides show the existence of more than one cationic conformer in equilibrium in the liquid state using Raman spectroscopy, and two polymorphs have been structurally characterised in the solid state.[9–12] In parallel to the empirical studies, computational studies have been rapidly developing for pure ionic liquids, focusing primarily on the 1-alkyl-3-methylimidazolium cation with alkyl chains of different length, which indicated the existence of two distinct domains, one made up of the positively charged imidazolium rings and the anions, that form a 3-D polar network held together by electrostatic interactions, and another non-charged region containing the neutral nonpolar groups, whose aggregation is controlled by short range van der Waals interactions.[2,13,14] Although our understanding of these relatively simple ionic liquids is now reaching maturity, our insight into binary systems is still in its infancy.[15]

All ionic liquids absorb water from the atmosphere. Although the ionic liquids range from hydrophobic to hydrophilic, they are all to some degree hygroscopic.[16–19] The presence of even small amounts of water in ionic liquids has a profound effect on their bulk physical properties (especially viscosity, density and conductivity),[17,20] and upon their application as solvents, whereas Rivera-Rubero and Baldelli studied the influence of water on the surface properties using surface-sensitive vibrational spectroscopy.[21] Aqueous solutions of 1-alkyl-3-methylimidazolium ionic liquids show clear evidence of aggregation and micelle formation when the alkyl group is octyl or longer; shorter chains produce less well defined systems. The systems have been studied by means of NMR and fluorescence spectroscopies, surface tension, conductivity and small angle neutron scattering (SANS) measurements.[22,23] Additionally, molecular dynamics (MD) simulations showed the significant nanostructural organisation in 1-octyl-3-methylimidazolium nitrate ionic liquid–water mixtures.[24] A simulation study of 1,3-dimethylimidazolium salts of chloride and hexafluorophosphate in water was carried out to investigate the microscopic

[a] *Dipartimento di Chimica, Università di Roma, La Sapienza, P. le Aldo Moro 5, I-00185 Roma, Italy. E-mail: umme.salma@uniroma1.it, lorenzo.gontrani@uniroma1.it*
[b] *Dipartimento di Scienze Chimiche e Geologiche – Università degli Studi di Cagliari, Cittadella Universitaria di Monserrato, S.P. 8, I-09042 Monserrato, Italy*
[c] *QUILL, The Queen's University of Belfast, Stranmillis Road, Belfast, Northern Ireland BT9 5AG, UK*

† Electronic supplementary information (ESI) available. See DOI: 10.1039/c6cp06860j

physical properties as a function of composition. This study indicated that at low concentrations of water, the water molecules remain isolated, whilst at higher concentrations, the water molecules form a network.[25] This self-aggregation of water molecules at different molar fractions was correlated to the ionic liquid organisation into a polar network by a Raman and FTIR study.[26] Vibrational spectroscopy was also used to investigate the structural changes in alkylimidazolium ionic liquids when mixed in water.[27] Using molecular simulations, the solubility of water was studied qualitatively.[28] Greaves *et al.* investigated the effect of different solutes on the nanostructure of protic ionic liquids having alkylammonium cations and nitrate and methanoate as anion, using small angle and wide angle X-ray scattering.[29] The effect of nonpolar solvent like alkanes on the nanostructure of an alkylphosphonium ionic liquid was recently investigated by Liang *et al.* who observed shifts in the position of SAXS prepeaks.[30] The position of scattering peaks and anti-peaks has been used to discuss the length scale of positive–negative and polar–apolar alternation.[31,32]

Recently, we have reported experimental studies on a series of four alkylammonium alkanoate ionic liquids, with varying alkyl chain lengths on the cation and the anion, using small and wide X-ray scattering (S-WAXS). The structural organisations in these systems have been discussed with reference to prepeak Q values, alkyl chain lengths on the cation and the anion, and also on anion type.[18] In this article, the structural organisation of butylammonium butanoate, $[CH_3CH_2CH_2CH_2NH_3][O_2CCH_2CH_2CH_3]$, abbreviated here as $[N_{0\ 0\ 0\ 4}][C_3CO_2]$, as a pure liquid and in mixtures with water, is explored using small angle and wide angle X-ray diffraction, and the results are interpreted with molecular dynamics simulations. The change in the nanostructure of $[N_{0\ 0\ 0\ 4}][C_3CO_2]$, as signalled by the first sharp diffraction peak (FSDP) at small Q values, depends significantly upon the concentration of water added.

Experimental

Starting materials

Butylammonium butanoate, $[N_{0\ 0\ 0\ 4}][C_3CO_2]$, was synthesised by a method described elsewhere.[18,33] Once prepared, the ionic liquid was dried by repeated freeze–drying cycles (checking the water content by Karl Fischer titration on each cycle) until no further decrease in the water content was observed (typically <500 ppm). The resulting butylammonium butanoate, $[N_{0\ 0\ 0\ 4}][C_3CO_2]$ (98% yield) is an extremely hygroscopic light yellow liquid; therefore it was kept under a dry N_2 atmosphere, in the glove box, until use. After removal from the glove box, the measured aliquots of water were added to produce eight solutions, whose mole fractions are reported in Table 1.

X-ray scattering

About 0.5 ml of liquid was introduced in amorphous quartz capillary (2 mm radius), which was afterward sealed with a Teflon band and kept in dry atmosphere, just before the measurements.

Table 1 Compositions of the simulated $[N_{0\ 0\ 0\ 4}][C_3CO_2]$–water mixtures

Mixture	χ_{water}	N_{IL}	N_{water}
χ_0[a]	0	435	0
χ_1	0.118	450	60
χ_2	0.352	423	230
χ_3	0.391	408	260
χ_4	0.573	400	536
χ_5	0.609	375	585
χ_6	0.723	350	924
χ_7	0.795	325	1300
χ_8	0.904	225	2131

[a] χ_0 to χ_8 indicate $[N_{0\ 0\ 0\ 4}][C_3CO_2]$–water mixtures with given χ_{water}, water mole fraction, N_{IL} and N_{water} are number of ion pairs of $[N_{0\ 0\ 0\ 4}][C_3CO_2]$ and number of water molecules, respectively; χ_0 corresponds to the neat ionic liquid.

The X-ray experiment (S-WAXS) was carried out on a Bruker D8 Advance with DaVinci design diffractometer (angle dispersive) equipped with a Mo KαX-ray tube (λ = 0.7107 Å), whose radiation was focused onto the sample with Göbel mirrors. The 2θ angle range available was 2.75–142° with a step of 0.25° within the Bragg–Brentano para-focusing geometry. The scattered intensity was gathered with the Lynxeye XE Energy-Dispersive 1-D detector.

After the corrections for background and sample absorption and the subtraction of the independent atomic scattering that does not depend on the structure $\left(\sum_{i=1}^{N} x_i f_i(Q)^2\right)$ from raw data (I_{EXP}), the "total static structure function" $I(Q)$ is obtained (eqn (1)):

$$I(Q) = I_{EXP}(Q) - \sum_{i=1}^{N} x_i f_i(Q)^2 \quad (1)$$

The structure function is the structurally sensitive part of the scattering intensity, and originates from the interference contributions from different atoms; the variable Q is the magnitude of the transferred momentum, and depends on the scattering angle (2θ), according to the relation $Q = 4\pi[\sin(\theta/\lambda)]$. Furthermore, the function $I(Q)$ is related to the partial radial distribution functions $g(r)$'s descriptive of the structure and obtainable from molecular simulations, on the basis of the following equation:

$$I(Q) = \sum_{i=1}^{N}\sum_{j=1}^{N} x_i x_j f_i f_j 4\pi\rho_0 \int_0^{q_{max}} r^2\left(g_{ij}(r) - 1\right)\frac{\sin(Qr)}{Qr}\mathrm{d}r \quad (2)$$

In the formulae above, x_i and x_j are the numerical concentrations of the species, f_i and f_j are their Q-dependent X-ray scattering factors respectively, and ρ_0 is the bulk number density. Eqn (2) is thus the link between experimental and model data.

Both the experimental and the theoretical structure functions were multiplied by a sharpening function $M(Q)$, necessary to improve the curve resolution at high Q, and then Fourier-transformed in the distance domain, according to the relation

$$\mathrm{Diff}(r) = \frac{2r}{\pi}\int_0^{\infty} QI(Q)M(Q)r\sin(Q)\mathrm{d}Q \quad (3)$$

In the differential correlation form of the total radial distribution (eqn (3)), only the structural contributions are present,

since the "uniform" contribution is left out. For a comprehensive report of all the formulas, see ref. 34 and 35.

Summarizing, the analysis of both reciprocal space ($I(Q)$) and distance space (Diff(r)) functions is used to compare X-ray experimental data and simulations. This methodology has been successfully applied to the study of molecular[36,37] and ionic liquids,[38,39] as well as solutions.[40,41]

Molecular dynamic simulations

Simulations were performed describing the potential energy with the two-body generalized amber force field (GAFF)[42] using the Amber/PMEMD v.12 package[43] as a molecular dynamics engine.

The four-site TIP4P model[44] was used to describe water, since it was previously found to give the best agreement with EDXD patterns. All parameters are reported in the ESI.†

The electrostatic interactions were modelled using the partial atomic charges obtained from restrained electrostatic potential (RESP) fitting[45] of the electrostatic potential for isolated cations and anions at the equilibrium geometry calculated at the B3LYP/6-31G* level. The initial configurations were generated randomly with the software Packmol,[46] using a minimum interatomic separation of 2 Å as a constraint. The cubic boxes used all had an initial edge of 50 Å and were filled with the necessary numbers of ions/water molecules, based on the value of experimental density. The length of the edge was chosen as twice the average largest correlation distance of these systems, which was identified in the last detectable peak in the experimental Diff(r) distributions and falls at about 25 Å.

The compositions of the ionic liquid–water mixtures are defined in terms of the mole fraction of water, χ_{water}, and are given in Table 1.

The simulation protocol can be summarised as follows:

- Energy minimisations were performed using both steepest descent and conjugated gradient methods.
- A short *NVT* run (20 ps) at 50 K.
- Gradual heating at 298 K in the *NPT* ensemble using the Berendsen weak coupling algorithm,[47] with external pressure set at 1 atm, followed by 2 ns *NPT* equilibration at 298 K. Coupling constants of 1 ps were used for both pressure and temperature.
- Productive *NVT* simulation for 2 ns with an integration time step of 2 fs, with trajectories collected every 1000 steps.

The trajectories were processed with in-house codes (X-ray patterns) and with ATEN software.[48]

Results and discussion

Aggregation in ionic liquids is a phenomenon by which either or cations or anions, or both, interact together, in solution or in the pure liquid, to form separated microphases that differ by charge and hydrophobicity. The recurrent separation of these domains is often described in terms of a mesoscopic order that is established in the system. The average repetitive distances between the phases of such an arrangement give rise to such distinctive diffraction peaks. The study of the peak positions as a function of the mixture composition can be used to understand the effect of different cations and anions and of the alkyl chains attached to either the ammonium or carboxylate moieties. In the Q range 0.25–2.75 Å^{-1}, which is dominated by intermolecular interactions, $[N_{0\,0\,0\,4}][C_3CO_2]$ shows a sharp pre-peak at $Q = 0.52$ Å^{-1}, that is attributable to the presence of comparatively longer alkyl chains (butyl) in both cation and anion causing the substantial segregation between these nonpolar moieties. In Fig. 1 (top), the position of the peak is shifted towards smaller Q values as the mole fraction of water is increased. The opposite effect was observed on the principal peak, as it moves towards larger Q values, Fig. 1 (bottom). This effect complies with our previous results on alkanoates[18] and with older measurements reported by Russina *et al.*[49]

The radial distribution function (RDF) corresponds to the probability density of finding a particle at the distance r from another centre (site) or particle taken as a reference. This radially averaged local organisation is one of the important characteristics of the local structures of dense fluids, and is linked to the effective interaction between pairs, *i.e.*, the potential of mean force (PMF), between two species. The local environment around a site or atom j can be properly represented by the coordination number, $N_{ij}(r)$, which is the average

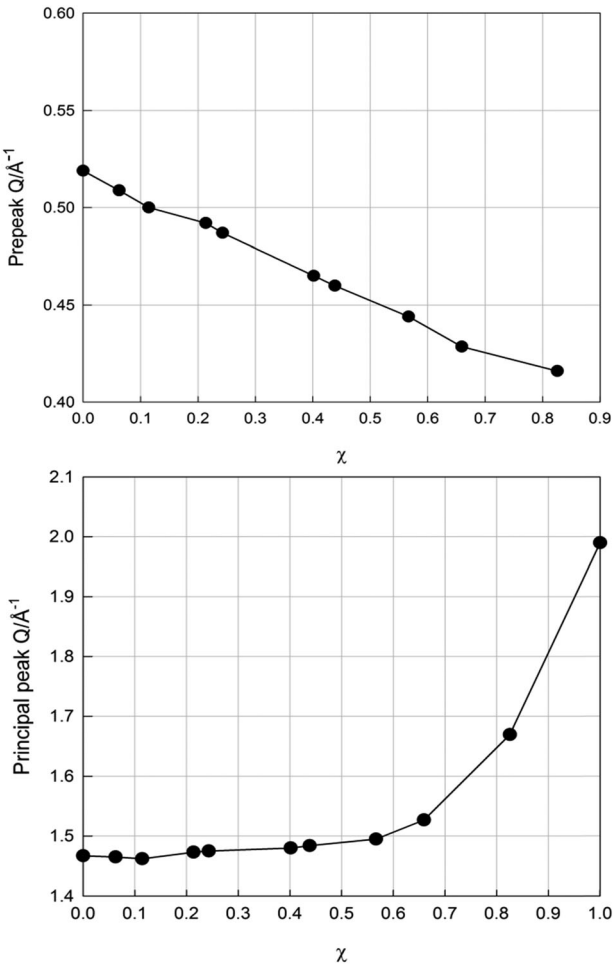

Fig. 1 Positions of pre-peaks (top) and principal peaks (bottom) for $[N_{0\,0\,0\,4}]$-$[C_3CO_2]$–water mixtures with increasing mole fraction of water, χ.

number of the site or atom i within a sphere of radius r around j, calculated by the integral of RDF.

Table 2 Experimental and theoretical densities for the $[N_{0\,0\,0\,4}][C_3CO_2]$–water system

Mixture	Experimental densities/g cm^{-3}	Theoretical densities/g cm^{-3}
χ_0	0.92886	0.9399
χ_1	0.93121	0.9499
χ_2	0.93947	0.9589
χ_3	0.94107	0.9590
χ_4	0.95136	0.9752
χ_5	0.95420	0.9767
χ_6	0.96482	0.9918
χ_7	0.97414	0.9984
χ_8	0.99345	1.0298

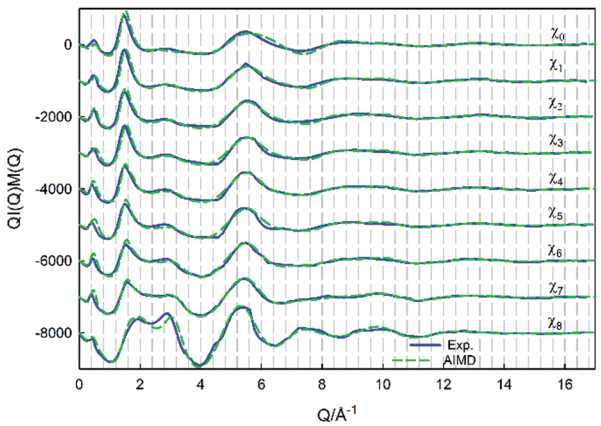

Fig. 2 Structure functions $QI(Q)M(Q)$ for neat $[N_{0\,0\,0\,4}][C_3CO_2]$ and its mixtures with water (see Table 1), dotted lines (green) represent MD while solid lines (blue) show experimental results.

The experimental densities of the liquid mixtures and the pure compound were measured, at 298.15 K and 0.1 MPa, by means of a vibrating tube densitometer (model DMA 4500 ME-Anton Paar-Gratz, Austria). Accuracy in the temperature was better about ±0.01 K. Density precision and accuracy was $\pm 1 \times 10^2$ and $\pm 5 \times 10^2$ kgm^{-3}, respectively. The "theoretical" densities of the present calculations (*i.e.* the simulation box densities obtained at the end of the *NPT* phase) and the experimentally determined values are not in exact agreement, but the theoretical data are *ca.* 1–3% higher (see Table 2). As there was reasonable agreement, the cell volume was not adjusted in the production phase.

The structure factor $QI(Q)M(Q)$ and radial distribution function Diff(r), derived from the SWAXS measurements for $[N_{0\,0\,0\,4}][C_3CO_2]$ in its neat state and its mixtures with water, are shown in Fig. 2 and 3.

The chain lengths on the cation and anion contain similar number of carbon atoms, perhaps permitting interdigitation and as a result, segregation. The alkyl chains in the aggregates observed are roughly longitudinal and polar heads of cations and anions may be located alternatively. The "effective" correlation distance, $d1$, obtained using Bragg's law, is considered to give the distance between the two polar head groups, and hence to give a measure of the domain sizes which generate the first sharp diffraction peak (FSDP), or pre-peak. This peak is observed in ionic liquids containing alkyl chains of two or more carbon atoms.[29]

In Fig. 2, it can be seen that the intensity of the pre-peak decreases with increasing water content (from top to bottom), becoming very small for χ_8 (which corresponds to a dilute aqueous solution of a salt). This phenomenon is possibly associated with the penetration of the water molecules into a segregated domain of apolar chains, which might lead to the reduction of the nanostructural organisation which is responsible for the existence of the pre-peak. A more likely interpretation is that

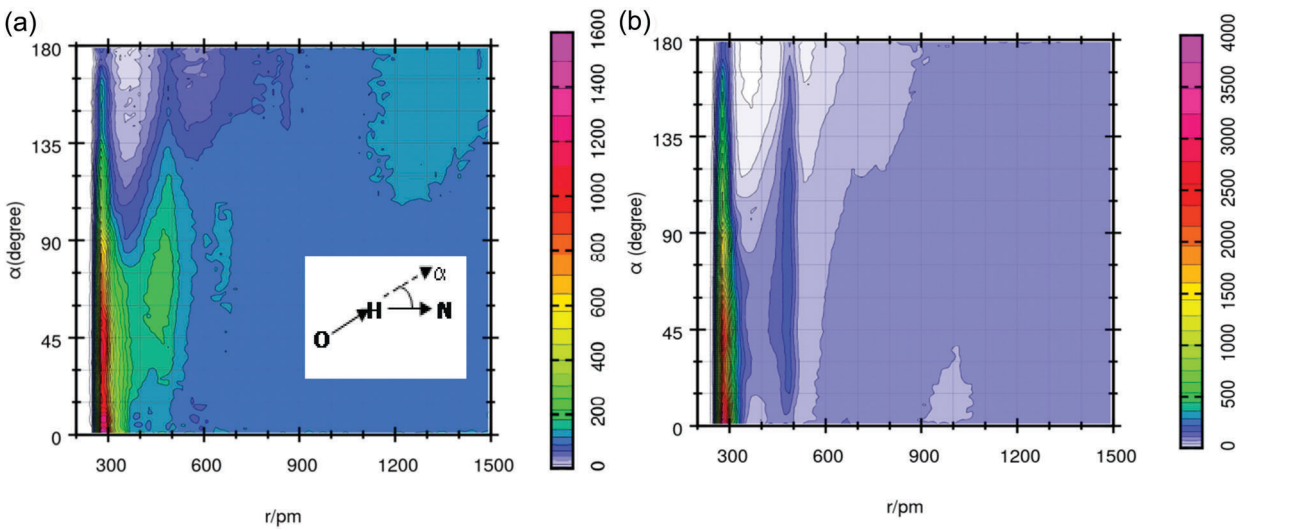

Fig. 3 Combined distribution functions extracted from the theoretical model which give the angular distribution of the cation–anion interaction (angle α, as shown in the inset) as a function of the donor–acceptor distance (N–O) for (a) neat $[N_{0\,0\,0\,4}][C_3CO_2]$, and (b) its mixture in water at maximum water concentration where the ions of IL are surrounded by water.

the water forms hydrogen bonds with both the anion and the cation, increasing the anion–cation separation with increasing amounts of added water.

Radial distribution functions show that cations and anions are present in alternate form with strong interactions and so their alkyl chains are present at shorter distance, which results in sharp peaks at low Q values. Crystal structures of simple alkylammonium salts demonstrate unambiguously that the nature of the crystalline state is dominated by the topological matrix of interionic hydrogen bonds, and there is no obvious interdigitation of the alkyl chains when the alkyl group is shorter than pentyl. Of course, the electrostatic nature of the systems dictates charge alternation. As water is added to the system, the interaction between the ions is reduced, as the water molecules disrupt the hydrogen bonded structure of the ionic liquid. The water bonds strongly to both the cations and the anions, replacing one 3D structural hierarchy with another. This disrupts the structure to such an extent that the pre-peak eventually disappears. In Fig. 3, RDF between cations and anions indicates a strong interaction between them in the neat ionic liquid, and the addition of water weakens that interaction and increases the separation between the ions.

Fig. 4 illustrates the RDFs for water–cation and water–anion interactions. As would be expected, the greater charge density on the carboxylate group attracts water molecules more strongly than the more diffuse charge density on the cation, but both clearly interact with water. In Fig. 3(a), a combined rdf/adf related to the existence of hydrogen bonding between the protons on the cation and the oxygen atoms on the anion is shown. The distance and the (ESI†) angle between donor and acceptor groups (N(H)···O) are taken as contour plot coordinates. Additionally, in Fig. 3(b), the corresponding functions are plotted for the correlations between the protons on the cation and the oxygen of anion in the presence of an excess of water.

A more pictorial view of the structure can be obtained from the spatial distribution functions (SDF).[50] In Fig. 5, the preferred localization of water (yellow) and cation (blue) around an anion taken as reference is reported for χ_1 and χ_8, clearly suggesting the increasingly stronger water–anion correlation. The complete set of SDFs is available in the ESI† (Fig. S2).

A further analysis was carried out to quantify the extent of hydrogen bonds between cation and anion and cation/anion–water. Even this investigation indicates that the anion hydration is favoured (*i.e.* at the maximum water concentration χ_8 the most probable coordination is 4 water molecules per anion, and only 1.5 per cation); the cation–anion coordination is inversely proportional to water content, as expected. The full results are reported in the ESI† (Fig. S1).

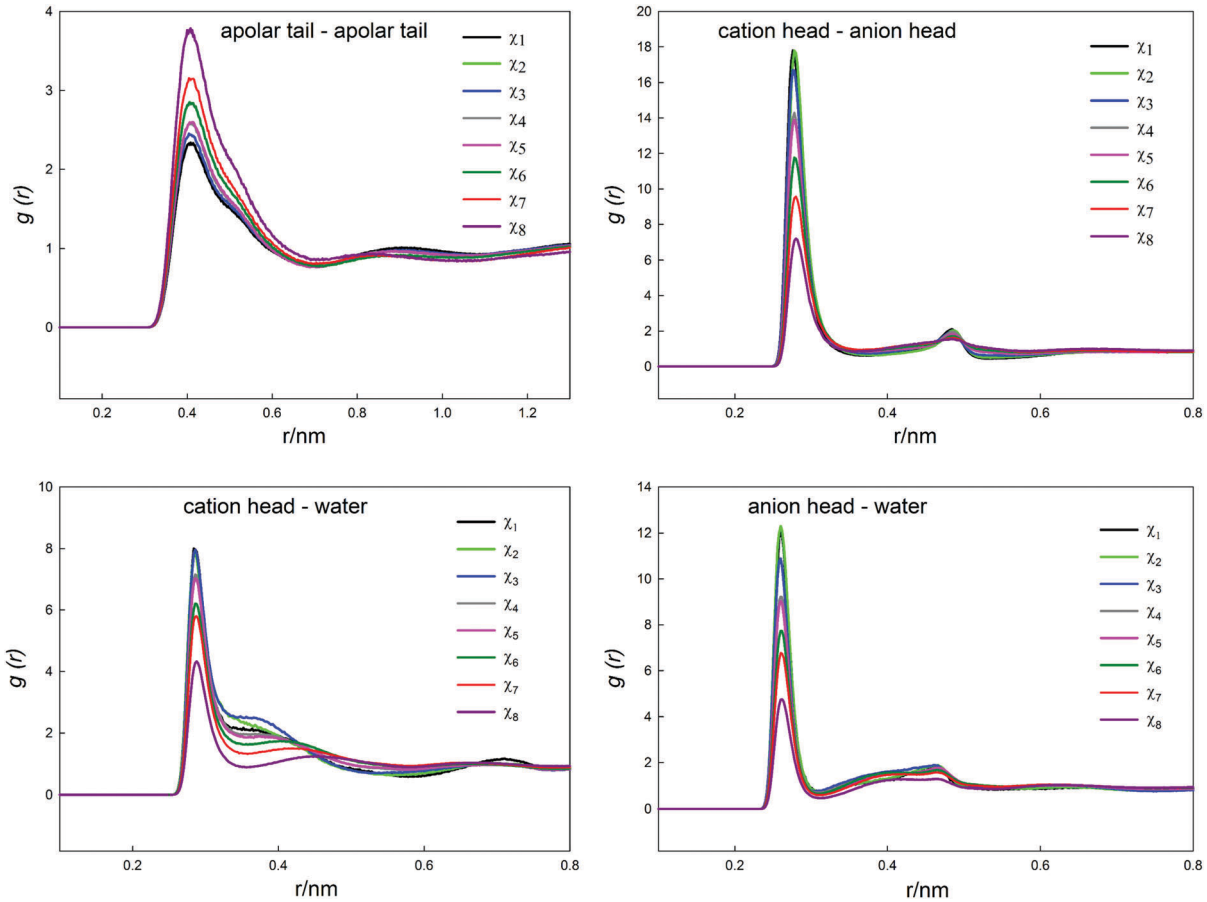

Fig. 4 Comparison between the interaction between apolar and polar groups of cation and anion of $[N_{0\ 0\ 0\ 4}][C_3CO_2]$ with water at different concentration.

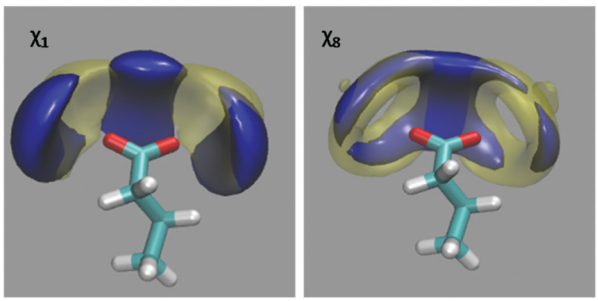

Fig. 5 Spatial distribution functions of atoms of cation and water around a butanoate anion. Clouds are plotted for an isosurface of cation (blue) and water (yellow) at least and most dilution.

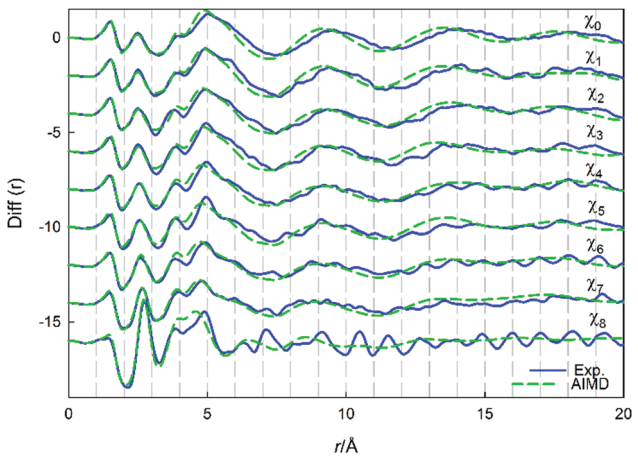

Fig. 6 Radial distribution function of neat $[N_{0\,0\,0\,4}][C_3CO_2]$ and its mixture in water with different mole fraction, solid line (blue) represents experimental while dotted line (green) shows MD results.

Turning to the X-ray scattering patterns (structure functions and Diff(r) functions), the experimental curves have been compared with those derived from MD simulations. $I(Q)$s are reported in Fig. 2, while Diff(r) functions are reported in Fig. 6. As it can be seen, the agreement is good over the whole Q range for $QI(Q)M(Q)$, indicating the reliable quality of the MD trajectories generated using the present interaction potential. The building up of water structure with increasing concentration can be distinctly appreciated in the Diff(r) curves, which point out the lowering of the first neighbour peak around 1.5 Å and the rise of the water oxygen–oxygen peak around 2.8 Å.

Summary

A pure ionic liquid, $[N_{0\,0\,0\,4}][C_3CO_2]$, and its various mixtures with water, were investigated by small and wide angle X-ray scattering. The disappearance of the pre-peaks with increasing concentration of water demonstrates the disruption of the hydrogen-bonded network of the ionic liquid. MD simulations were also performed, which gave good agreement with experimental results. The computed RDFs mapped the changes in structural features, as the ionic liquid was increasingly diluted with water, which showed a preferential attraction for the anion over the cation. Studies of longer chain cations and anions will clearly be of interest, and are currently underway in our groups.

Acknowledgements

NVP and KRS thank the industrial advisory board of QUILL for their support. The authors thank the Department of Chemistry, "La Sapienza" University of Rome, for providing free computing time on NARTEN Cluster HPC Facility.

References

1 M. Deetlefs, M. Fanselow and K. R. Seddon, *RSC Adv.*, 2016, **6**, 4280–4288.
2 J. N. Canongia Lopes, M. C. Gomes and A. A. H. Pádua, in *Ionic Liquids Completely UnCOILed: Critical Expert Overviews*, ed. N. V. Plechkova and K. R. Seddon, Wiley, Hoboken, New Jersey, 2015, pp. 83–106.
3 C. Hardacre, C. Mullan and T. G. A. Youngs, in *Ionic Liquids Completely UnCOILed: Critical Expert Overviews*, ed. N. V. Plechkova and K. R. Seddon, Wiley, Hoboken, New Jersey, 2015, pp. 55–82.
4 J. N. A. Canongia Lopes and A. A. H. Pádua, *J. Phys. Chem. B*, 2006, **110**, 3330–3335.
5 E. Bodo, L. Gontrani, R. Caminiti, N. V. Plechkova, K. R. Seddon and A. Triolo, *J. Phys. Chem. B*, 2010, **114**, 16398–16407.
6 C. M. Gordon, J. D. Holbrey, A. R. Kennedy and K. R. Seddon, *J. Mater. Chem.*, 1998, **8**, 2627–2636.
7 C. J. Bowlas, D. W. Bruce and K. R. Seddon, *Chem. Commun.*, 1996, 1625–1626.
8 T. L. Greaves, D. F. Kennedy, S. T. Mudie and C. J. Drummond, *J. Phys. Chem. B*, 2010, **114**, 10022–10031.
9 H. O. Hamaguchi and R. Ozawa, in *Advances in Chemical Physics*, ed. S. A. Rice, 2005, vol. 131, pp. 85–104.
10 K. Nishikawa, S. L. Wang, H. Katayanagi, S. Hayashi, H. O. Hamaguchi, Y. Koga and K. I. Tozaki, *J. Phys. Chem. B*, 2007, **111**, 4894–4900.
11 S. Saha, S. Hayashi, A. Kobayashi and H. Hamaguchi, *Chem. Lett.*, 2003, **32**, 740–741.
12 J. D. Holbrey, W. M. Reichert, M. Nieuwenhuyzen, S. Johnston, K. R. Seddon and R. D. Rogers, *Chem. Commun.*, 2003, 1636–1637.
13 E. I. Izgorodina, in *Ionic Liquids UnCOILed: Critical Expert Overviews*, ed. N. V. Plechkova and K. R. Seddon, Wiley, Hoboken, New Jersey, 2013, pp. 181–230.
14 Y. Zhang and E. J. Maginn, *Phys. Chem. Chem. Phys.*, 2014, **16**, 13489–13499.
15 H. Niedermeyer, J. P. Hallett, I. J. Villar-Garcia, P. A. Hunt and T. Welton, *Chem. Soc. Rev.*, 2012, **41**, 7780–7802.
16 L. Cammarata, S. G. Kazarian, P. A. Salter and T. Welton, *Phys. Chem. Chem. Phys.*, 2001, **3**, 5192–5200.
17 K. R. Seddon, A. Stark and M.-J. Torres, *Pure Appl. Chem.*, 2000, **72**, 2275–2287.

18 U. Salma, P. Ballirano, M. Usula, R. Caminiti, N. V. Plechkova, K. R. Seddon and L. Gontrani, *Phys. Chem. Chem. Phys.*, 2016, **18**, 11497–11502.
19 Y. Kohno and H. Ohno, *Chem. Commun.*, 2012, **48**, 7119–7130.
20 U. Schröder, J. D. Wadhawan, R. G. Compton, F. Marken, P. A. Z. Suarez, C. S. Consorti, R. F. de Souza and J. Dupont, *New J. Chem.*, 2000, **24**, 1009–1015.
21 S. Rivera-Rubero and S. Baldelli, *J. Am. Chem. Soc.*, 2004, **126**, 11788–11789.
22 M. Blesic, M. H. Marques, N. V. Plechkova, K. R. Seddon, L. P. N. Rebelo and A. Lopes, *Green Chem.*, 2007, **9**, 481–490.
23 J. Bowers, C. P. Butts, P. J. Martin, M. C. Vergara-Gutierrez and R. K. Heenan, *Langmuir*, 2004, **20**, 2191–2198.
24 W. Jiang, Y. T. Wang and G. A. Voth, *J. Phys. Chem. B*, 2007, **111**, 4812–4818.
25 C. G. Hanke and R. M. Lynden-Bell, *J. Phys. Chem. B*, 2003, **107**, 10873–10878.
26 B. Fazio, A. Triolo and G. Di Marco, *J. Raman Spectrosc.*, 2008, **39**, 233–237.
27 Y. Jeon, J. Sung, D. Kim, C. Seo, H. Cheong, Y. Ouchi, R. Wawa and H. O. Hamaguchi, *J. Phys. Chem. B*, 2008, **112**, 923–928.
28 J. Deschamps, M. F. C. Gomes and A. A. H. Padua, *ChemPhysChem*, 2004, **5**, 1049–1052.
29 T. L. Greaves, D. F. Kennedy, N. Kirby and C. J. Drummond, *Phys. Chem. Chem. Phys.*, 2011, **13**, 13501–13509.
30 M. Liang, S. Khatun and E. W. Castner Jr., *J. Chem. Phys.*, 2015, **142**, 121101.
31 H. K. Kashyap, J. J. Hettige, H. V. R. Annapureddy and C. J. Margulis, *Chem. Commun.*, 2012, **48**, 5103–5105.
32 K. B. Dhungana, L. F. O. Faria, B. Wu, M. Liang, M. C. C. Ribeiro, C. J. Margulis and E. W. Castner, Jr., *J. Chem. Phys.*, 2016, **145**, 024503.
33 M. Usula, N. V. Plechkova, A. Piras and S. Porcedda, *J. Therm. Anal. Calorim.*, 2015, **121**, 1129–1137.
34 R. Caminiti, M. Carbone, G. Mancini and C. Sadun, *J. Mater. Chem.*, 1997, **7**, 1331–1337.
35 D. A. Keen, *J. Appl. Crystallogr.*, 2001, **34**, 172–177.
36 L. Gontrani, F. Ramondo, G. Caracciolo and R. Caminiti, *J. Mol. Liq.*, 2008, **139**, 23–28.
37 L. Gontrani, F. Ramondo and R. Caminiti, *Chem. Phys. Lett.*, 2006, **417**, 200–205.
38 M. Campetella, L. Gontrani, E. Bodo, F. Ceccacci, F. Marincola and R. Caminiti, *J. Chem. Phys.*, 2013, **138**(18), 184506.
39 L. Gontrani, P. Ballirano, F. Leonelli and R. Caminiti, in *The structure of Ionic Liquids*, ed. R. Caminiti and L. Gontrani, Springer International Publishing, Switzerland, 2014, pp. 1–37.
40 A. Mariani, R. Dattani, R. Caminiti and L. Gontrani, *J. Phys. Chem. B*, 2016, **120**, 10540–10546.
41 M. Usula, F. Mocci, F. Cesare Marincola, S. Porcedda, L. Gontrani and R. Caminiti, *J. Chem. Phys.*, 2014, **140**, 124503.
42 J. M. Wang, R. M. Wolf, J. W. Caldwell, P. A. Kollman and D. A. Case, *J. Comput. Chem.*, 2004, **25**, 1157–1174.
43 D. A. Case, J. T. Berryman, R. M. Betz, D. S. Cerutti, T. E. Cheatham, T. A. Darden III, R. E. Duke, T. J. Giese, H. Gohlke, A. W. Goetz, N. Homeyer, S. Izadi, P. Janowski, J. Kaus, A. Kovalenko, T. S. Lee, S. LeGrand, P. Li, T. Luchko, R. Luo, B. Madej, K. M. Merz, G. Monard, P. Needham, H. Nguyen, H. T. Nguyen, I. Omelyan, A. Onufriev, D. R. Roe, A. Roitberg, R. Salomon-Ferrer, C. L. Simmerling, W. Smith, J. Swails, R. C. Walker, J. Wang, R. M. Wolf, X. Wu, D. M. York and P. A. Kollman, *AMBER 2015*, University of California, San Francisco, 2015.
44 W. L. Jorgensen, J. Chandrasekhar, J. D. Madura, R. W. Impey and M. L. Klein, *J. Chem. Phys.*, 1983, **79**, 926.
45 P. Cieplak, W. D. Cornell, C. Bayly and P. A. Kollman, *J. Comput. Chem.*, 1995, **16**, 1357–1377.
46 L. Martínez, R. Andrade, E. G. Birgin and J. M. Martínez, *J. Comput. Chem.*, 2009, **30**, 2157–2164.
47 H. J. C. Berendsen, J. P. M. Postma, W. F. Vangunsteren, A. Dinola and J. R. Haak, *J. Chem. Phys.*, 1984, **81**, 3684–3690.
48 M. Brehm and B. Kirchner, TRAVIS – A free Analyzer and Visualizer for Monte Carlo and Molecular Dynamics Trajectories, *J. Chem. Inf. Model.*, 2011, **51**(8), 2007–2023.
49 O. Russina, B. Fazio, G. D. Marco, R. Caminiti and A. Triolo, *The structure of Ionic Liquids*, ed. R. Caminiti and L. Gontrani, Springer International Publishing, Switzerland, 2014, pp. 53–78.
50 A. P. Lyubartsev and A. Laaksonen, *J. Biomol. Struct. Dyn.*, 1998, **16**(3), 579–592.